JOURNAL OF GAS TECHNOLOGY

Volume 10 / Issue 1 / Summer 2025 / Pages 69-86

Journal Home page: https://jgt.irangi.org

Selective Removal of Sulfur Dioxide from Oxygen Using Porous Iron: A Molecular Dynamics Study

Mostafa Jafari[1], Mohammad Mahdi Yousefi[2], Ali Vatani[3*], Roozbeh Sabetvand[4]

1. Researcher, Institute of Liquefied Natural Gas (I-LNG), School of Chemical Engineering, College of Engineering, University of Tehran, Tehran, Iran
2. M.Sc. Student, Institute of Liquefied Natural Gas (I-LNG), School of Chemical Engineering, College of Engineering, University of Tehran, Tehran, Iran
3. Full Professor, Institute of Liquefied Natural Gas (I-LNG), School of Chemical Engineering, College of Engineering, University of Tehran, Tehran, Iran
4. Ph.D. Graduate, Department of Physics and Energy Engineering, Amirkabir University of Technology, Tehran, Irann

ARTICLE INFO

ORIGINAL RESEARCH ARTICLE

Article History:
Received: 18 June 2025
Revised: 26 August 2025
Accepted: 07 September 2025

Keywords:
O_2/SO_2 separation
Molecular dynamics
Gas purification
Membrane technology
Permeability
Perm-selectivity
Porous iron membrane
Atomic-scale purification

DOR: 20.1001.1/jgt.2025.2072087.1061

ABSTRACT

Sulfur dioxide (SO_2) is a toxic pollutant generated primarily by the combustion of sulfur-containing fossil fuels, and its removal is crucial for sustainable industrial development. In this computational study, molecular dynamics (MD) simulations were employed to evaluate a porous iron membrane for separating oxygen from a SO_2 gas stream. The Fe membrane was modeled with the Embedded Atom Method (EAM), while the O_2-SO_2mixture was described using the DREIDING force field. Equilibration confirmed the structural stability of the atomic models, reflecting appropriate MD settings and carefully chosen initial conditions. To characterize separation performance, we report SO_2 and O_2 sorption coefficients, gas-membrane interaction energies, and the membrane's post-separation mechanical properties. The simulations further show that the initial conditions (e.g., temperature and pressure) govern the perm-selective behavior of the porous iron membrane throughout the simulation campaign. Under optimized conditions, the membrane achieved an O_2 purity of ~81% and an O_2 recovery of 96.7% in the designed atomic-scale purification system. This performance arises from optimum interaction between the porous iron membrane and target gas molecules. Numerically, the magnitude of the interaction energy between these modeled samples increased to -83.14 eV. This described procedure did not disturb the mechanical performance of the designed porous membrane, and the ultimate strength and Young's modulus of them reached 212.39 MPa and 6.00 GPa (respectively) after the gas molecules selective removal process was fulfilled.

How to cite this article
M. Jafari, M.M. Yousefi, A. Vatani, R. Sabetvand, Selective Removal of Sulfur Dioxide from Oxygen Using Porous Iron: A Molecular Dynamics Study. Journal of Gas Technology. 2025; 10(1): 69-86. (https://jgt.irangi.org/article_731528.html)

* Corresponding author.
E-mail address: avatani@ut.ac.ir, (A. Vatani).

Available online 22 September 2025

1. Introduction

SO_2 is a noticeable atmospheric constituent, particularly during and after volcanic eruptions, and it contributes to acid rain and secondary particulate formation (Fioletov, McLinden et al. 2020, Li, Li et al. 2022). From a mitigation standpoint, sulfur can be removed from fuels upstream of combustion to suppress SO_2 formation, while downstream, refineries commonly employ the Claus process for sulfur recovery (Pourfayaz, Kazempour et al. 2025). In parallel, chelated-iron redox systems remain essential options for treating sulfur-bearing gas streams (Wei, Wu et al. 2024). Beyond air-quality concerns, SO_2 exposure is linked to adverse human-health outcomes, and elevated atmospheric concentrations can also perturb plant physiology and ecosystem functioning. Accordingly, purifying oxygen from SO_2-containing streams is of practical relevance to environmental protection and industrial sustainability (Pasichnyk, Stanovskay et al. 2023).

Building on early PVDF hollow-fiber studies, recent work has demonstrated that hydrophilic membrane contactors operated with alkaline absorbents (e.g., NaOH) can selectively remove SO_2 under flue-gas and marine-engine conditions (Xu, Huang et al. 2020). Complementary CFD-based analyses have compared prevalent liquid absorbents within hollow-fiber modules, clarifying how gas/liquid velocities and solvent selection govern SO_2 uptake (Cao, Taghvaie Nakhjiri et al. 2023). Comprehensive reviews further position membrane contactors as compact, energy-lean alternatives to conventional scrubbers for SO_2 and related acid gases, and summarize module design, wetting control, and scale-up considerations (Pasichnyk, Stanovsky et al. 2023). These insights motivate the use of tailored polymeric or ceramic hollow-fiber modules and properly chosen absorbents to enhance SO_2 removal while preserving oxygen in the treated stream. The implemented absorbent liquids were constituted of water-based solutions of NaOH, K_2CO_3, alkanolamines, and Na_2SO_3, flowing in the lumen side of the HF sample under a laminar regime. The simultaneous membrane absorption of SO_2/CO_2 molecules was estimated using an aqueous Na_2SO_3 mixture, and their selective removal was appropriately detected. This suggests that the atomic matrix absorption technique offers an energy-saving method for eliminating SO_2 from flue-based compounds.

(Gao, Qiu et al. 2018) highlighted a novel concept for the practical implementation of SO_2 molecule absorption in a hydrophilic ceramic matrix that indicated promising thermal/mechanical performance. These researchers studied the behavior of SO_2 molecule absorption into a NaOH solution in a hydrophilic alumina (Al_2O_3) matrix contactor, focusing on the removal ratio and mass transfer flux of SO_2 molecules. Their results indicated that the hydrophilic membrane matrix was more competitive when using a NaOH concentration higher than 0.2 mol. L^{-1} value. They concluded that the hydrophilic α-Al_2O_3 matrix shows long-term physical stability under 480 h of continuous performance. Subsequent studies have refined the mass-transfer picture in tubular hydrophilic ceramic modules and confirmed the role of operating conditions and absorbent selection in governing SO_2 uptake and selectivity.

(Kong, Qiu et al. 2019) reported a group of hydrophobic tubular asymmetric ceramic-based matrices for the SO_2 molecule elimination process. They observed that most of the SO_2 molecules' mass transfer resistance existed in the atomic matrix phase, indicating that optimizing the matrix parameters, rather than operational conditions, should be the primary consideration to improve the overall pollution transfer behavior. Furthermore, they noted that the SO_2 pollution separation efficiency depended negligibly on the atomic pore radii inside the membrane (matrix). Still, it

could be significantly enlarged by optimizing the thickness and inner size of matrix tubes. Accordingly, when comparing structural classes used for gas purification, metallic and metal-based porous matrices offer attractive attributes that make them suitable supports or active media for acid-gas treatment.

More than polymeric and ceramic matrices, a porous metallic system exhibits strong performance in gas molecule adsorption due to its combination of high surface area, tunable pore structure, and chemically active metallic sites that enhance host-guest interactions (Xinyao, Jiang et al. 2025). The interconnected pores provide extensive pathways for gas diffusion and adsorption. At the same time, the metallic framework offers sites for van der Waals, electrostatic, or even chemisorptive interactions depending on the gas species. In metallic materials, design flexibility allows control over pore size, distribution, and surface functionality to achieve selective and reversible gas adsorption under varying conditions. The adjustable geometry and electronic environment of metal nodes enable enhanced binding affinity and regeneration capability, which are crucial for applications in gas separation, purification, and storage. Thus, through coordinated pore engineering and metal center functionalization, porous metallic matrices maintain high adsorption capacity, fast diffusion rates, and molecular selectivity in both single- and multi-component gas systems (Jiang, C et al. 2022).

Iron and iron-oxide surfaces, in particular, exhibit strong interactions/sensitivity to SO_2, as shown by surface-science studies and gas-sensor evaluations (e.g., thin iron-oxide films and iron-oxide nanorods)(Nguyen, Luong et al. 2021, Soldemo and Weissenrieder 2021). In parallel, hydrophilic hollow-fiber membrane contactors operated with alkaline absorbents (e.g., NaOH) have demonstrated selective SO_2 removal under flue-/flue-/marine-relevant conditions, underscoring the role of robust inorganic (metal/ceramic) matrices in harsh environments (Kong, Gong et al. 2020, Xu, Huang et al. 2020). The sensitivity of metallic structures to gas separation refers to their ability to selectively separate specific gases from a gaseous mixture, such as O_2 or SO_2, from SO_2-O_2 mixtures. Porous metal membranes provide a large surface area to volume ratio, contributing as an exciting option for industrial separations. In contrast, polymeric membranes possess both chemical and thermal stability issues. Nevertheless, at the moment, no commercial porous metallic membranes are available, but there is significant interest in exploring their potential for gas separation. This is the main reason why, in this study, the investigation of porous iron membranes for SO_2/O_2 separation is proposed, considering that iron oxides and their nanocomposites have proven to be effective gas sensing materials in gas and biosensors (Singh, Saxena et al. 2021). The porous metallic materials are commonly processed using powder metallurgy, casting, and deposition techniques (Dukhan, Chen-Wiegart et al. 2020).

Hence, this work aims to describe the absorption process of SO_2 molecules by using a porous iron membrane, which represents a new option in this area. In addition to conventional experimental methods, computer simulations can be used effectively to study the behavior of atomic membranes in adsorbing SO_2molecules. One of the most common methods for computer simulations is the Molecular Dynamics (MD) approach (Ma, Hua et al. 2022, Liao, Wen et al. 2024). In this method, the time evolution of atoms is predicted by using the Newton equation. Here, the purification process of O_2 molecules via a metallic matrix was studied using the MD method, and the effects of temperature and pressure changes on the process performance were examined for the first time. Computationally, temperature, total energy, SO_2 molecules absorption ratio, interaction energy, ultimate strength, and

Young's Modulus have been calculated in the MD simulation box. In actual cases, porous metallic membranes are vital in modern air purification due to their exceptional mechanical strength, corrosion resistance, and precise control of pore size, which enable effective removal of fine particulates, aerosols, and gaseous pollutants under various temperature and pressure conditions. So, outputs of current research can be applied in actual cases.

2. Development of MD Calculations

In this computational study, a porous iron membrane was brought into contact with an O_2-SO_2 gas mixture to probe SO_2 sorption and oxygen separation. After model construction, 10-ns production runs were performed to quantify sorption metrics and assess separation performance. All simulations were carried out with LAMMPS(Plimpton 1995, Brown, Wang et al. 2011, Thompson, Aktulga et al. 2022). The porous Fe membrane and the O_2-SO_2 mixture were modeled at the atomistic level as Fe, O, and S species (see Figure 1), and structures were visualized/analyzed using OVITO (Stukowski 2009). Periodic boundary conditions were applied along the x and y axes. In contrast, fixed boundaries were imposed along z to confine transport across the membrane Systems were equilibrated in the isothermal-isobaric (NPT) ensemble at T = 300 K and P =1 bar using standard Nosé-Hoover-type algorithms(Martyna, Tobias et al. 1994).

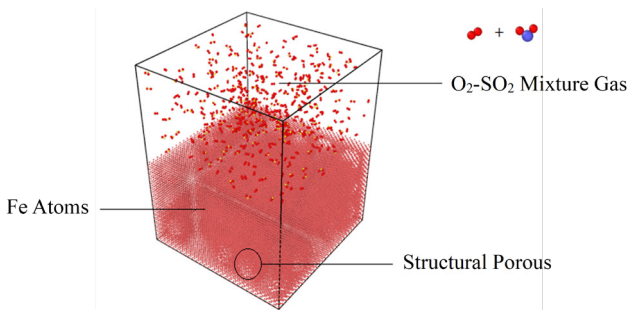

Figure 1. Schematic of atomic structures arrangement in the MD simulation box by using the LAMMPS package

The MD simulation is a prevailing tool to explore the dynamics of nanostructures based on Newton's laws for various phenomena(Haile 1992, Sadus 2002), such as air purification. It has the capability of tracing the behavior of atomic membranes in various pollution filtering. Conventionally, these simulations define the particle trajectories by solving Newton's equation, considering the forces among multiple atoms. The atomic arrangement was used to describe the behavior of the porous iron membrane under various initial conditions. Considering the importance of interatomic potential in MD simulation results, the DREIDING force field has been applied in the atomic description of the O_2-SO_2 gas mixture (Mayo, Olafson et al. 1990). As reported in previous research, the use of this force field is appropriate for gas molecule simulations in various conditions (Dokyr, D et al. 2018). This simulation setting allowed the structural stability and actual interaction between different molecules to be observed over time. Lennard-Jones (LJ) potential has been used to compute the atomic interaction among multiple structures in this force field (Gao, Ji et al. 2018),

$$\phi(r_{ij}) = 4\varepsilon\left[\left(\frac{\sigma}{r_{ij}}\right)^{12} - \left(\frac{\sigma}{r_{ij}}\right)^{6}\right] \qquad r_{ij} \le r_c \qquad (1)$$

ε defines the depth of the LJ well, sigma indicates the finite distance at which the LJ is zero, and the distance between various particles specified by rij parameter. In equation (1), rc (cut-off radius) is chosen 12 Å in all of our simulations. The bonded potential is made up of the simple strength and angle bend components. In the DREIDING force field, the simple strength is defined by a linear oscillator with the following formalism (Li 2014),

$$E = \tfrac{1}{2}\, k_r\, (r\text{-}r_0)^2 \qquad (2)$$

where the kr is indicated as the linear oscillator constant, the atomic bond length is shown by r_0. Moreover, equation (3) represents

the angle bend in SO_2 molecules through an angular oscillator (Li 2014):

$$E = ½\ k_\theta\ (\theta\text{-}\theta_0)^2 \quad (3)$$

Where k_θ represents the angular oscillator constant, and θ_0 indicates the equilibrium degree of the angle contact. Numerically, in the defined force field, the r_0 of O/O and S/O interactions are equal to 1.31 Å and 1.69. Also, θ_0 of O/S/O interaction is equal to 92.10 (Mayo, Olafson et al. 1990). The other atomic interaction parameters for various molecules in the O_2-SO_2 gas mixture are represented in (Table 1) (Mayo, Olafson et al. 1990). The porous iron matrix, consisting of Fe atoms, is described by the Embedded Atom Model (EAM). In the previous report, this force field effectively describes the time evolution of metallic atoms within the computational box. It facilitates the detection of thermodynamic stability in the designed Fe-based system (Han, B et al. 2025). This interatomic potential is defined as follows (Daw and Baskes 1984, Daw, Foiles et al. 1993):

$$\mathrm{E_i} = \mathrm{F_\alpha}\left(\sum_{\mathrm{i\neq j}} \rho_\beta(\mathrm{r_{ij}})\right) + \frac{1}{2}\sum_{\mathrm{j\neq i}} \varphi_{\alpha\beta}(\mathrm{r_{ij}}) \quad (4)$$

Where F constant is the embedding energy as a function of the atomic electron density ρ, φ is the pair potential interaction, and α and β are the element types of atoms i and j.

Table 1: The ε and σ constants for LJ formalism in DREIDING force-field (Mayo, Olafson et al. 1990)

Element	σ(Å)	ε(kcal/mol)
O	0.415	3.71
S	0.305	4.24
Fe	0.055	4.54

The potential of atom-based compound $V(r^N)$ is assumed for each pair of atoms. Computationally, it can be defined $V(r^N)$ for atomic systems with N atoms as reported below (Rapaport 2004),

$$V\left(r^N\right) = \Sigma\sum_{i<j} V\left(r_{ij}\right) \quad (5)$$

After defining the potential parameter for nanostructures inside the MD box, the simulation process was completed. To describe the atomic displacement, Newton's equation at the nanometric level is set as the gradient of the atom-based potential (force-field) (Rapaport 2004),

$$F_i = \sum_{i\neq j} F_{ij} = m_i \frac{d^2 r_i}{dt^2} = m_i \frac{dv_i}{dt} \quad (6)$$

$$F_{ij} = -grad\ V_{ij} \quad (7)$$

From equations (6) and (7), the momentum Pi can be defined as in the following (Rapaport 2004),

$$P_i = m_i\, v_i \quad (8)$$

Hence, the Energy (E) of the atomic structures can be expressed in the form of the Hamilton equation (9),

$$\mathrm{H}\left(r,P\right) = \frac{1}{2m}\sum_i P_i^2 + V\left(r_1 + r_2 + \ldots + r_n\right) = E \quad (9)$$

The velocity-Verlet approach is applied to estimate the particle's time evolution, considering the integration form of Newton's law in equations (10), and (11) (Verlet 1967, Hairer, Lubich et al. 2003, Press, Teukolsky et al. 2007),

$$r(t+\Delta t) = r(t) + v(t)\Delta t + \frac{1}{2}a(t)\Delta t^2 + \cdots \quad (10)$$

$$v(t) + \frac{a(t) + a(t+\Delta t)}{2}\Delta t + \cdots \quad (11)$$

In the equations above, r(t+Δt) and v(t+Δt) are the position and velocity of modeled atoms at any time (respectively), and r(t) and v(t) are the initial values. Theoretically, various

ensembles are implemented to create an initial condition inside the simulation box. In this work, the grand canonical ensemble was obtained by applying the Nosé-Hoover barostat, and thermal equilibrium was achieved by using the LAMMPS package (Nosé 1984, Hoover 1985). After the equilibrium process, the simulation continued for 10 ns later with the micro-canonical ensemble (Hilbert, Hänggi et al. 2014). According to the descriptions above, the computational studies were carried out as follows:

Step A: SO_2-O_2 gas mixture and the porous iron-based membrane were simulated with DREIDING and EAM force fields and equilibrated by NPT/NVT ensemble for 10000000 time steps with Δt = 1 fs. Using these ensembles caused the initial thermodynamic conditions implemented to design the atomic sample. For this purpose, the nuclear structure's initial temperature and initial pressure are set at T_0 = 300 K and P_0=1 bar (respectively) as initial conditions. Afterwards, atomic structures reached an equilibrium phase, and their stability is presented by total temperature and total energy calculations.

Step B: The atomic purification procedure was implemented to equilibrate structures for 10000000 time steps with the NVE ensemble. This ensemble caused the removal process to occur within a non-limiting computational box. For this purpose, SO_2 molecules are absorbed by the porous membrane in the MD simulation box. After this process, physical parameters such as SO_2 and O_2 absorption coefficients, interaction energy, and mechanical properties of the membrane after the separation procedure are reported to describe the atomic behavior of the porous iron membrane in the O_2 purification procedure. The MD simulation details are reported in (Table 2). All of the MD simulations were repeated 5 times with defined simulation settings, and the average value of the numeric outputs was reported.

Table 2: MD Simulation Details in Current Computational Research

Computational Parameter	Value/Setting
Computational Box Length	150×150×300 Å3
Boundary Condition	P-P-F
Initial Temperature	300 K
Initial Pressure	1 bar
Time Step	1 fs
Computational Algorithm	NPT
Temperature Damping Ratio	10
Pressure Damping Ratio	100
Equilibrium Time	10 ns
Total Simulation Time	20 ns
Number of Pollution Molecules	175

3. Result and Discussion

Firstly, the atomic behavior of the O_2-SO_2 gas mixture and the porous iron membrane were described at initial temperature and pressure (T_0 = 300 K and P_0 = 1 bar). The simulation results show the initial arrangement of atoms in the simulation box, adopted using the DREIDING and EAM functions. This atomic phase of simulated compounds is estimated by temperature and total energy calculation. The atom-based compound's temperature varied as a function of MD time steps, as reported in (Figure 2A). It illustrates that the atomic structures equilibrated after t =7 ns. Physically, this thermal equilibrium arises from the reduction of atomic oscillation by MD time, demonstrating the validity of the MD simulation settings (Asgari, Nguyen et al. 2020, Jolfaei, Jolfaei et al. 2020, Mosavi, Hekmatifar et al. 2020). Atomic oscillation reduction arises from the decrease

in atom mobility inside the computational box. This decrease, caused by the mean distance between various particles, did not significantly affect the structure, which was stabilized under defined conditions. Furthermore, (Figure 2B) displays the total energy variations in atomic systems as a function of MD simulation time. As shown in this figure, the total energy of the atomic structure converged after t = 7 ns to a constant value with a numerical range variation below 2%, which was considered acceptable. Numerically, the total energy of the porous iron membrane and the O_2-SO_2 gas mixture system reached -398.11 eV after 10 ns. Theoretically, this physical parameter has a reciprocal relation with the mean distance of atoms, and the target atomic structure stability was achieved by increasing the total energy magnitude. T_o ensure sufficient time in the equilibration phase, this simulation factor was increased to 20 ns. The total energy output in this simulation was -398.13 eV, which did not significantly vary from the energy value after 10 ns. This energy output indicated that the 10 ns were sufficient time to observe the thermodynamic equilibrium in the modeled structure, which arises from the proper matching of the interatomic force field and the atomic positions. Next, to validate the MD simulation results in the current atom-based study, the Radial Distribution Function (RDF) of O atoms in the O_2 gas system was also calculated. The RDF of simulated structures can describe their atomic arrangement. Computationally, the RDF function is defined by g(r), a parameter showing the probability of finding an atom at a finite distance from other atoms (neighbor atoms). This output is a characteristic property of the atomic system, consistent with the previous structural report (Okwuashi 2020). Physically, this consistency arises from the compliance between the modeled structure and the simulation settings, as validated by current MD simulations. (Figure 3) shows this output (RDF results of O atoms in O_2 gas structure).

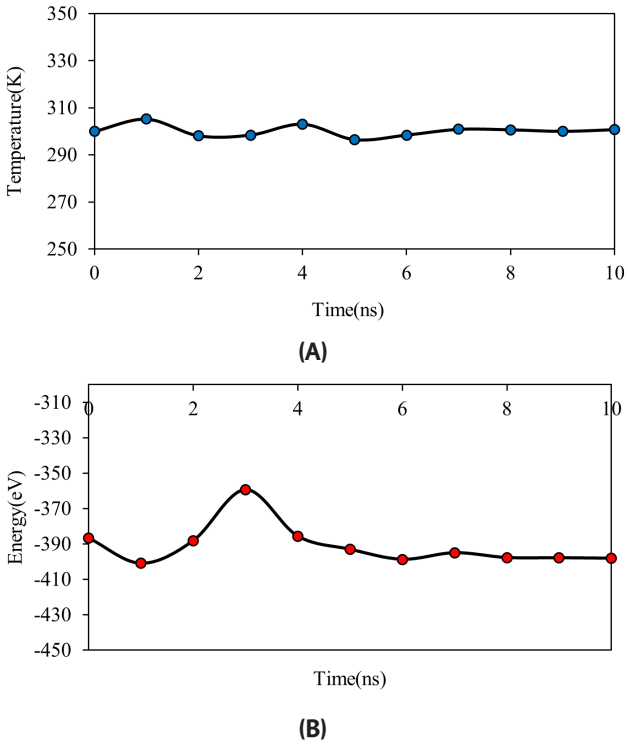

Figure 2. Temperature And B) Total Energy Variation of Porous Iron Membrane and O_2- SO_2 Gas Mixture System as A Function of Defined MD Time Steps (Time)

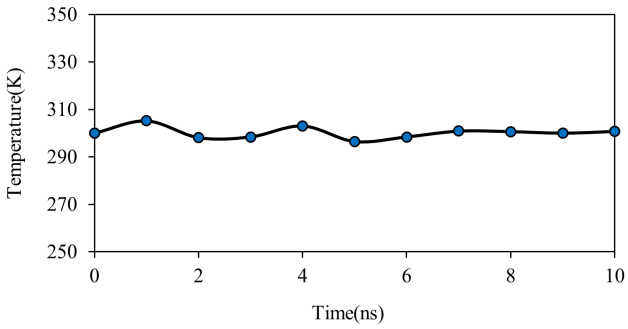

Figure 3. The Oxygen-Oxygen Radial Distribution Function (RDF) of O_2 Gas at T_0 = 300 K And P_0 = 1 Bar (As an Initial Condition)

As soon as the equilibrium procedure was achieved, the atomic evolution was implemented to the O_2-SO_2 system, with ensemble change from NPT to NVT for t =10 ns. This computational step indicated the

purification process of O_2 molecules from the O_2-SO_2 gas system, as shown in (Figure 4). After gas molecules diffused into the pristine matrix, potential energy was generated within the final system. This evolution caused gas molecule fluctuations to decrease inside the matrix, completing the air purification procedure.

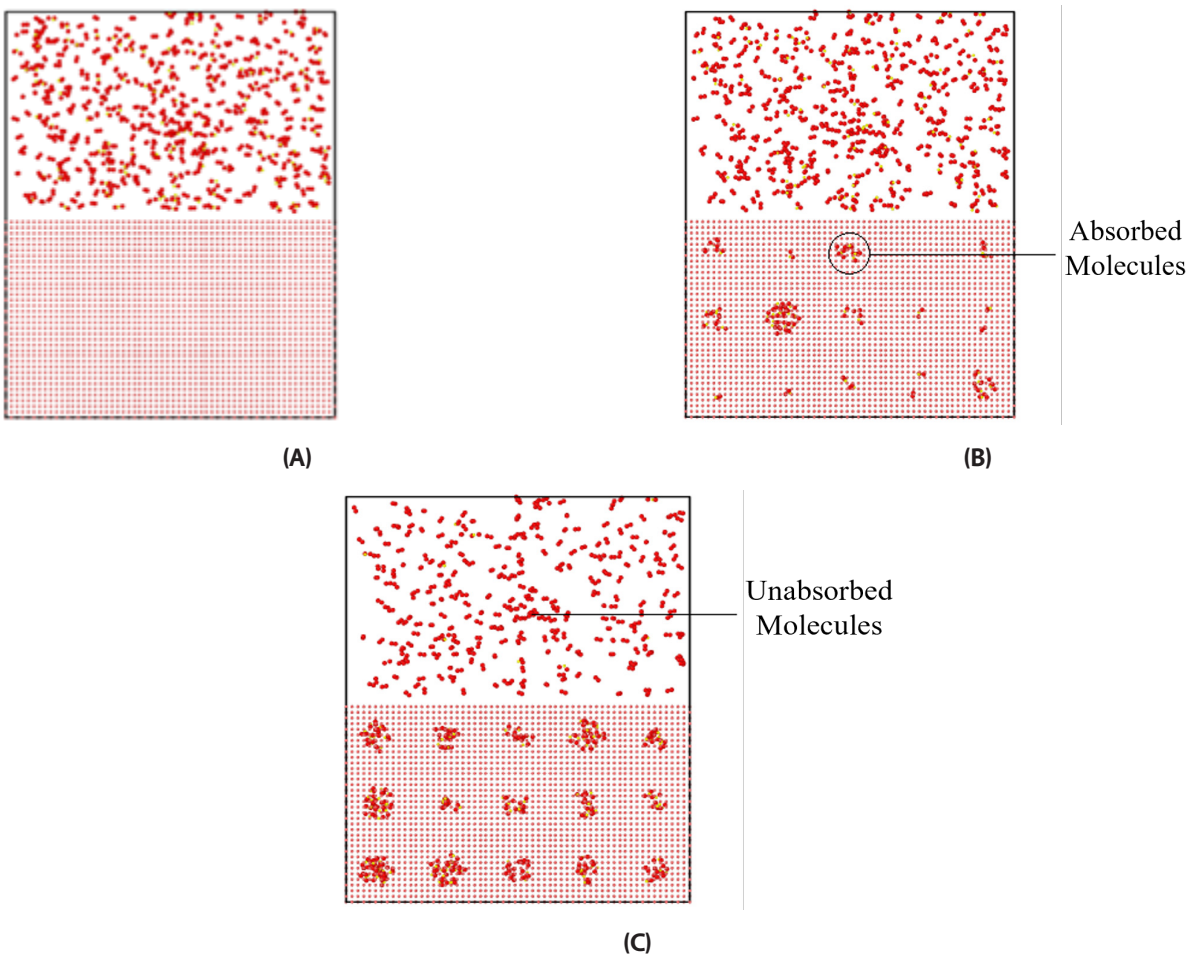

Figure 4. Time Evolution of O_2 Gas Purification Process from SO_2 Molecules as Pollution with Porous Iron Membrane After A) 0, B) 5000000, And C) 10000000 Time Steps

The number of absorbed SO_2 molecules (with porous iron matrix) changed as a function of MD time, as shown in (Figure 5). As displayed in this figure, the computational time steps are sufficient for detecting the oxygen purification process at the initial conditions. After detecting the atomic process, the number of O_2 molecules absorbed by the porous membrane was calculated. Numerically, the number of SO_2 molecules that diffused inside the atomic matrix converged to 133 molecules after 10 ns. By this atomic absorption ratio, the efficiency of the defined membrane is around 76%, indicating the appropriate performance of the metallic membrane for air purification purposes. Furthermore, the computed value of absorbed O_2 molecules, which diffused into the pristine membrane, was equal to 21, while the O_2 molecule adsorption ratio was negligible. To calculate these parameters, the evolution of each particle (atoms/molecules) inside the computational box was estimated with Newton's second law equation, which was introduced in the "development of MD calculations" section. Then, the number of target molecules which trapped within the metallic matrix is counted.

This computational approach predicted the recovery ratio of O_2 molecules in the designed system, converging to 95.3% after 10 ns. Computationally, the number of O_2 molecules in the target region (outside the membrane) is counted to estimate the recovery ratio.

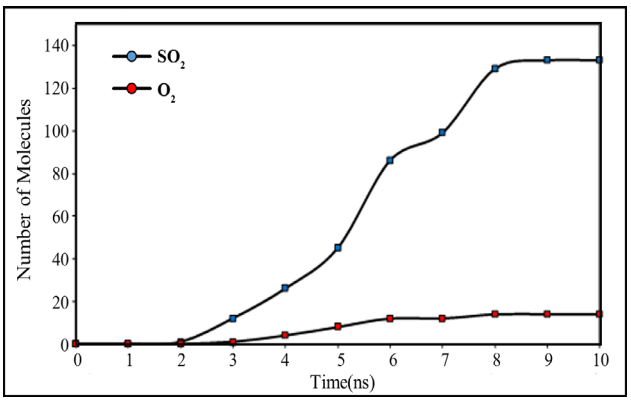

Figure 5. The Number of SO_2 And O_2 Molecules Trapped in Porous Regions of Iron-Based Membrane as A Function of MD Time

Physically altering the initial condition, the atomic resonance within the samples was significantly affected, and their structural unity converged to new states. In this section, the effects of initial conditions in the O_2 gas purification process are described. The MD simulations indicated that the atomic interaction between the porous iron membrane and SO_2 molecules decreased as the initial temperature or pressure increased, leading to a decrease in the efficiency of the metallic membrane in the air purification process. These atomic evolutions arise from changes in the mean distance and atomic force between various particles inside the computational box. The increase in temperature and decrease in pressure caused the mean velocity of particles inside the computational box to increase, leading to more effective collisions between them. These interactions caused the diffusion ratio of molecules to increase, leading to more molecules being adsorbed onto the porous iron matrix. The pressure increase has the opposite effect on atomic system evolution, and the adsorption of target molecules occurs with more precision. This behavior caused the separation efficiency to increase at higher pressures instead of lower levels. Thus, the temperature increase or pressure decrease in the air purification process can disrupt this phenomenon. MD outputs predicted molecules' mobility changes at defined conditions. (Figures 6,7) show the number of O_2 and SO_2 molecules, which were absorbed by iron-based membranes as a function of MD simulation time. Numerically, the number of absorbed O_2 and SO_2 molecules inside the porous iron matrix converged to 142 and 10 molecules, respectively, by creating optimized conditions in the MD simulation box. As reported before, this optimized condition was created by decreasing the temperature and increasing the pressure for t = 10 ns.

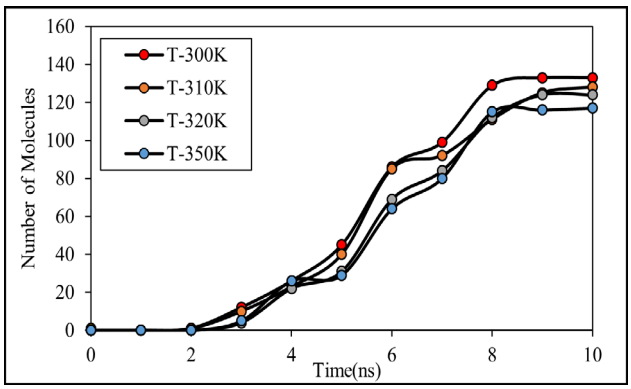

(A)

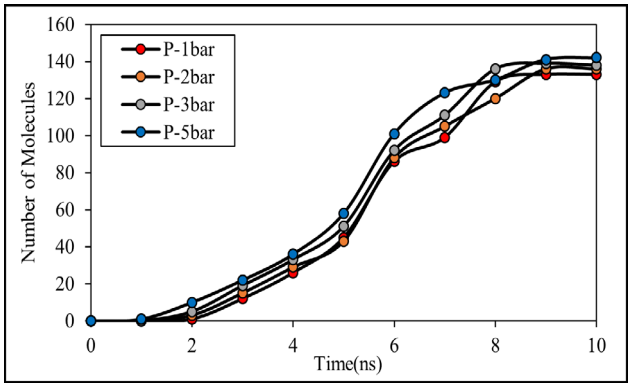

(B)

Figure 6. The Number of Absorbed SO_2 Molecules with Porous Iron Membrane as Defined by Initial A) Temperature and B) Pressure

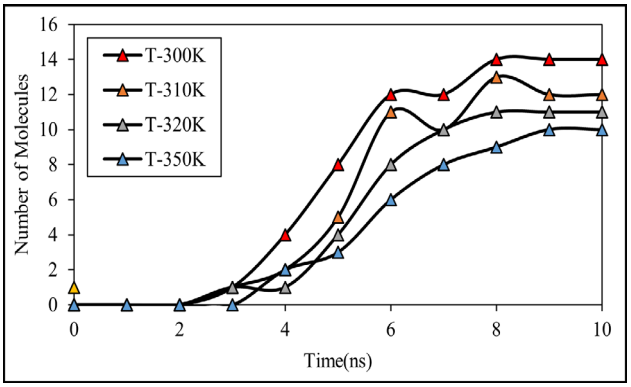

(A)

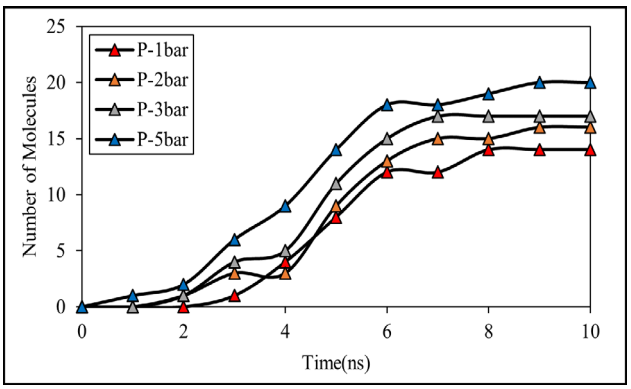

(B)

Figure 7. The Number of Absorbed O_2 Molecules with Porous Iron Membrane as A Function of Initial A) Temperature and B) Pressure

The O_2 molecules recovery ratio and permeability changed as a function of initial temperature and pressure, as depicted in (Figure 8). Numerically, the O_2 molecules recovery ratio varied from 93.3% to 96.7% according to defined systems. Hence, these results predicted that the atomic interaction between the O_2-SO_2 mixture and the membrane was significantly affected by changes in operating conditions, which should be considered in actual applications. Furthermore, permeability value in modeled samples varied from 3.4×10-3 Barrer to 4.9×10-3 Barrer. This parameter refers to the ability of O_2 molecules to diffuse inside the membrane. The O_2 purification procedure was done effectively, depending on the decrease in permeability value in the designed porous iron membrane. The atomic interaction between the atomic membrane and the gas structure is another physical parameter that can describe the purification process of oxygen molecules. In this section, the atomic interaction between porous iron membrane and O_2-SO_2 mixture gas was calculated. Simulation outputs showed that, increasing temperature from T0 = 300 K to T0 = 350 K, the interatomic interaction energy changes from -75.22 eV to -69.01 eV between the atomic membrane and the gas system. Computationally, the interaction energy in modeled samples, which consists of the porous matrix and gas molecules, is calculated by the mutual potential energy between them. Hence, the simulation results predicted that the temperature increase caused effective collision among various particles and, randomly, their evolution decreased the efficiency of the modeled metallic membrane. A pressure increase from P_0 = 1 bar to P_0 = 5 bar causes this atomic parameter to enlarge from -75.22 eV to -83.14 eV. Physically, the increase of this parameter induces the enlargement of atomic absorption in simulated systems. This evolution can be described with the optimum atomic displacement of polluting molecules inside the modeled matrix. With the SO_2 molecules' absorption increase, the purification process occurs effectively. The interaction force between membrane and polluting molecules shows similar results, and this parameter changes from -18.93 eV/Å to 30.64 eV/Å as listed in (Table 3). Generally, the gas purification efficiency increases with a decrease in temperature and an increase/ pressure, consistent with previous reports for similar structures (Liu, Y et al. 2018, Hashmi, Moiz et al. 2024). This consistency arises from an appropriate time evolution description of the purification procedure by designed MD simulation, and we validated this procedure description in the current research.

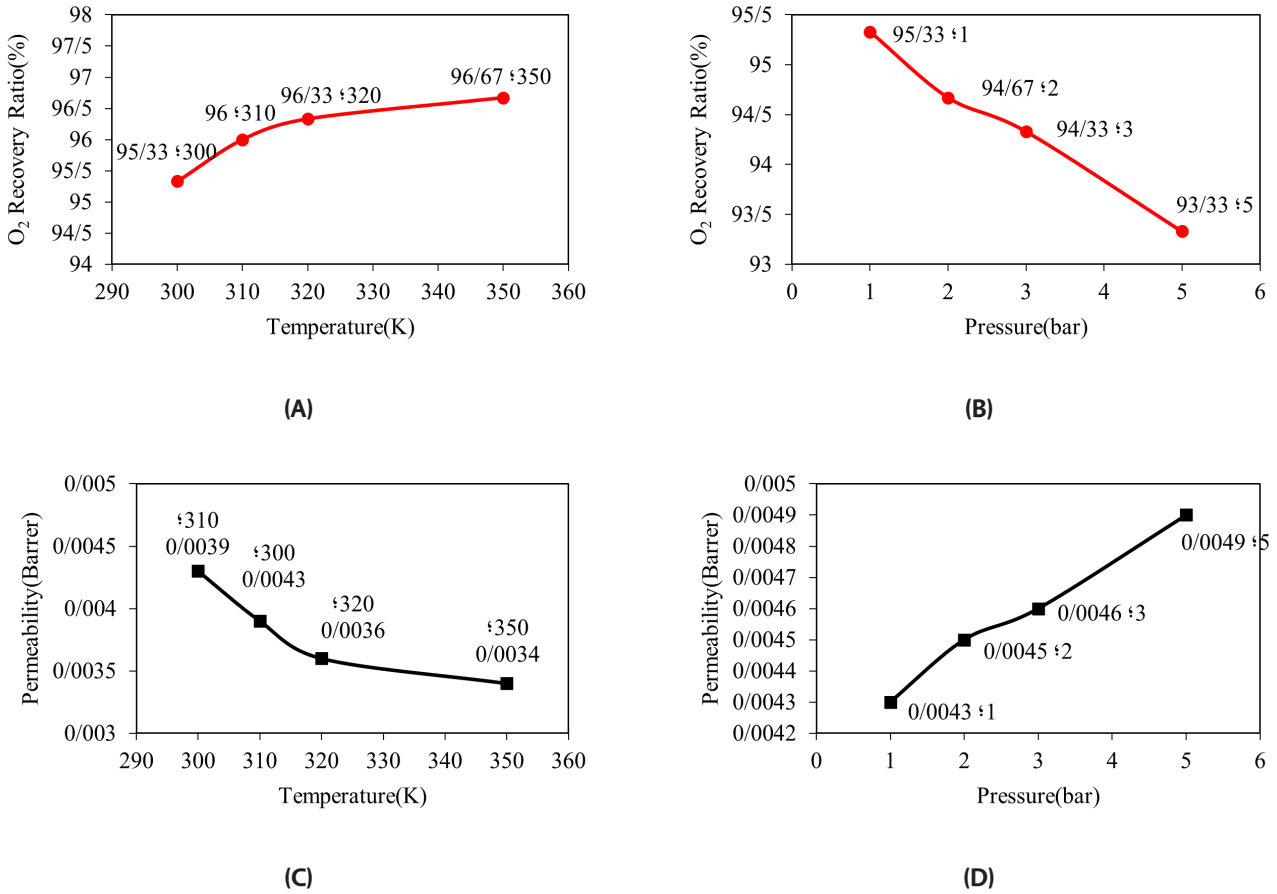

Figure 8. O_2 Molecules Recovery Ratio as a Function of Initial (A) Temperature and (B) Pressure. Permeability of O_2 Molecules as a Function of Initial (C) Temperature and (D) Pressure in the Current Computational Study

Table 3. The Numerical Outputs of MD Simulations in Current Research are Presented as a Function of Initial Temperature and Pressure

Initial Temperature (K) - Pressure (bar)	O_2 Molecules Number	SO_2 Molecules Number	Gas-Membrane Interaction Energy (eV)	Interaction/Force (eV/Å)	Purification Efficiency (%)
T_0=300 K - P0=1 bar	14	133	-75.22	-24.83	76.00
T_0=310 K - P0=1 bar	12	128	-73.29	-21.00	73.14
T_0=320 K - P_0=1 bar	11	124	-70.16	-19.11	70.86
T_0=350 K - P_0=1 bar	10	117	-69.01	-18.93	66.86
T_0=300 K - P_0=2 bar	16	136	-78.05	-26.68	77.71
T_0=300 K - P_0=3 bar	17	138	-82.21	-29.93	78.86
T_0=300 K - P_0=5 bar	20	142	-83.14	-30.64	81.14

The mechanical behavior of iron-based membranes is an important parameter for real-world applications. In the final step of our computational study, a cubic porous iron membrane was used to describe the mechanical properties of these atom-based samples. To report the mechanical performance of the designed membrane, the sample was structurally expanded by uniform intensity, and the interatomic stresses in various regions of the

sample were reported as the stress-strain curve.

The density parameter as a function of MD simulation time is shown in (Figure 9A). The convergence of the density parameter indicates that the simulated structure reaches equilibrium after t = 10 ns. This convergence results from the decrease in atomic fluctuations under the defined initial condition. Computationally, this atomic evolution was accessible by adopting position and interatomic potentials and simulating it as a function of time. For mechanical behavior analysis of the iron porous membrane, the external force was applied to the atomic matrix as depicted in (Figure 9B). The stress-strain curve was calculated to study the mechanical behavior of the iron-based membrane, before and after the purification process. Mechanical quantities such as the Young's modulus and the ultimate strength were estimated from the calculated curve. In (Figure 10), as the external force increases, the structures' deformation values are depicted, and, finally, the stress-strain curve is obtained using these values. The deformation process of an atomic sample will depend on its elastic modulus and geometry. The stress and strain calculations output of the mechanical test procedure was depicted in (Figure 11). The latter shows structural unity inside the atomic sample, which arises from the attraction force between various parts of the system. From our MD simulations, Young's modulus and ultimate strength of pure iron-based membrane are calculated as 6.93 GPa and 245.66 GPa, respectively. These computed values were comparable with previous studies about iron-based structures and validated our computational method in the current research (Kuhn and Medlin 2000).

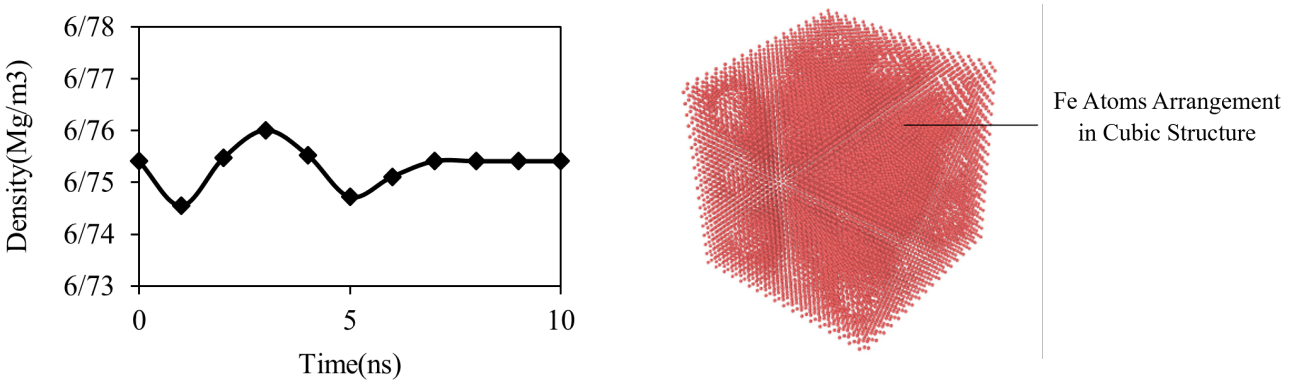

Figure 9. Mass Density Changes of Pure Porous Iron Matrix Arrangement as a Function of MD Time During the Equilibration Process (A), Schematic (B)

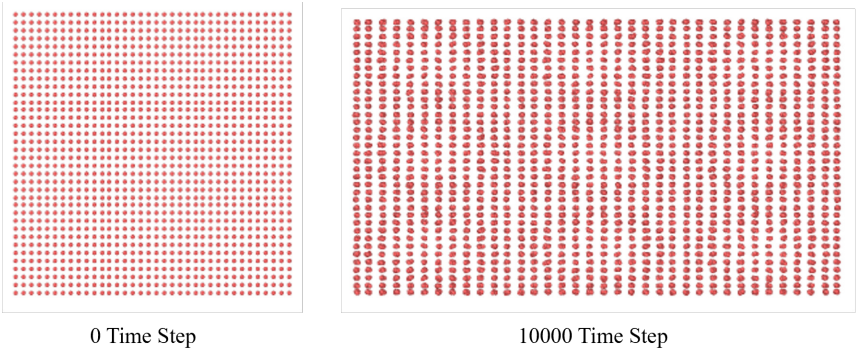

Figure 10. The Atomic Evolution of Pure Porous Iron Membrane at 0 and 10000 Time Steps of the Mechanical Deformation Process

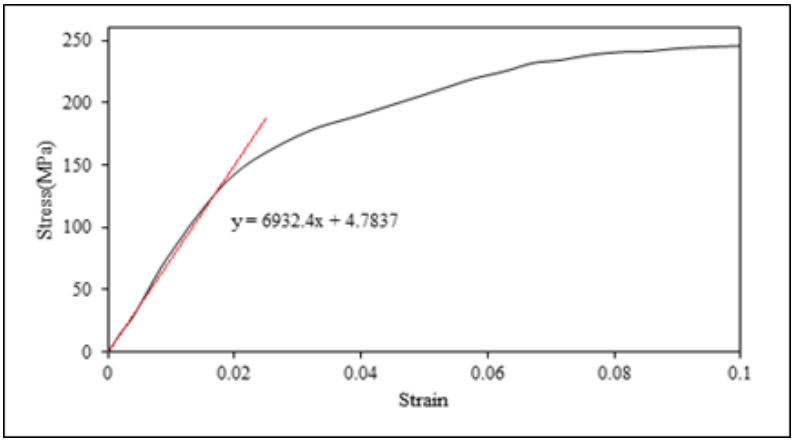

Figure 11. Stress-Strain and B) Young's Modulus Curves of the Pure Porous Iron Membrane Calculated by the Molecular Dynamics Approach

The absorption of SO_2 molecules should affect the mechanical properties of the pure metallic membrane. For this reason, the porous iron matrix's mechanical behavior after the purification process was estimated at T_0 = 300 K and P_0 = 1 bar as the initial condition. The results of the mechanical test of this atomic membrane after the purification process are shown in (Figure 12). After the atomic equilibration process at the initial condition, the metallic membrane was expanded to simulate the mechanical evolution with a 0.001 ps^{-1} strain ratio. The stress-strain curve of the porous iron membrane's deformation test in the Z direction is shown in (Figure 13). This mechanical estimation was calculated using the least-square formalism, implemented to reduce data errors. Numerically, by absorbing the mixture gas with the pure metallic structure, the mechanical-based quantities such as Young's modulus and ultimate strength decreased and converged to 6.00 GPa and 212.39 GPa, respectively, as listed in (Table 4). These results confirm the diffusion of SO_2 and O_2molecules into the porous iron membrane, weakening the membrane's mechanical performance. Physically, the diffusion of guest atoms inside the host metallic membrane increased the mean distance between various atoms. By this structural evolution, the interatomic force and structural unity decreased. The MD simulations obtained in this section should be considered in the design of porous iron-based membranes for gaining better commercial outputs. This describes the structural evolution and how gas molecules diffuse inside the pristine iron porous matrix without disturbing its thermodynamic stability. This behavior, detected by limitations in atomic fluctuation amplitude over time, verifies the designed system applications and should be considered in actual cases.

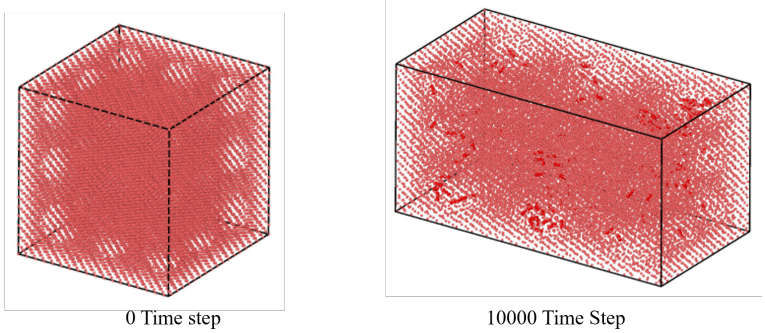

Figure 12. Schematic of Porous Iron Matrix in the Presence of Absorbed O_2 and SO_2 Molecules After the Mechanical Deformation Process

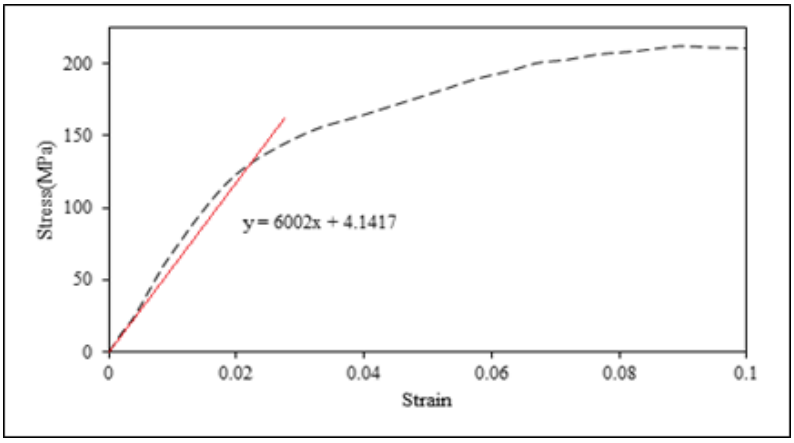

Figure 13. The Stress-Strain and Young's Modulus Curves of the Porous Iron Membrane After the O_2 Purification Process, Calculated by the MD Approach

Table 4. The Mechanical Properties of Various Simulated Metallic Membranes are Studied in the Current Computational Work

Atomic structure	Young's Modulus (GPa)	Ultimate Strength (MPa)
Pure Porous Iron Membrane	6.93	245.66
Porous Iron Membrane after the O_2 Purification process	6.00	212.39

4. Conclusion

In the present computational research, the molecular dynamics (MD) approach was used to describe the porous iron membrane performance for the oxygen purification process (in the presence of SO_2 molecules as pollutants). MD simulation results at defined initial conditions can be listed as follows:

A. The DREIDING and Embedded Atom Model (EAM) functions were adequate choices for the MD description of porous iron membrane and O_2-SO_2 gas system.

B. MD simulations indicated the number of oxygen and SO_2 molecules absorbed by the porous iron membrane is 12 and 128 molecules after 10 ns.

C. The increase in the initial temperature of simulated structures caused the accuracy to decrease, and the speed of the purification procedure improved. Numerically, by increasing the initial temperature to 350 K, the number of absorbed SO_2 molecules by the metallic membrane converged to 117.

D. Increasing the initial temperature of simulated structures caused an enlargement in the accuracy and performance speed of the purification procedure. Numerically, by initial pressure enlarging to 5 bar, the number of absorbed SO_2 molecules by the metallic membrane converged to 142 molecules.

E. The recovery ratio and permeability of O_2 converged to 96.7% and 3.4·10-3 Barrer, respectively, in our designed O_2 purification system.

F. Porous iron membrane was weakened mechanically after the purification process. Numerically, the ultimate strength of the pure metallic membrane decreased from 245.66 GPa to 212.39 GPa after O_2-SO_2 gas mixture absorption took place with them. Also, Young's modulus parameter decreased from 6.93 GPa to 6.00 GPa after the oxygen molecule purification process.

These MD simulation results showed that the atomic arrangement of Fe atoms in the porous iron membrane can be used for standard air purification procedures. Practically, these results can be implemented in various purification processes for optimizing the actual application efficiency.

Declarations

Author Contributions: Conceptualization, Mostafa Jafari; Formal analysis, Mostafa Jafari and Mohammad Mahdi Yousefi; Data curation, Mostafa Jafari; Writing - original draft, Mostafa Jafari, Mohammad Mahdi Yousefi, Roozbeh Sabetvand; Supervision, Ali Vatani.

Acknowledgments: Support from the LAMMPS Tube Center is gratefully acknowledged.

Funding N/A

Conflicts of interest / Competing interests: The authors declare that they have no conflicts of interest.

Availability of data and material: Data available on request from the authors.

Code availability: LAMMPS main inputs are available on request from the authors.

Nomenclature

Fij	Atomic force between i and j atoms
Vij	Potential energy between i and j atoms
m	Atomic mass
rc	Cut-off radius
rij	Atomic distance of i and j atoms
t	Time step in molecular dynamics simulation
T	Temperature in molecular dynamics simulation
v	Atomic velocity
a	atomic acceleration
$Natom$	Number of atoms
Nsf	Degree of freedom
kB	Boltzman constant
$r0$	Equilibrium bond length

Greek symbols

ε	Energy constant in Lennard-Jones function
σ	Length constant in Lennard-Jones function
$\theta 0$	Equilibrium angle
Δt	molecular dynamics time step
$F\alpha$	embedding energy in Embedded Atom Model
$\varphi\alpha\beta$	pair potential interaction in Embedded Atom Model

References

Asgari, A., Q. Nguyen, A. Karimipour, Q.-V. Bach, M. Hekmatifar and R. Sabetvand (2020). "Develop molecular dynamics method to simulate the flow and thermal domains of H_2O/Cu nanofluid in a nanochannel affected by an external electric field." International Journal of Thermophysics 41(9): 126. https://doi.org/10.1007/s10765-020-02708-6

Brown, W. M., P. Wang, S. J. Plimpton and A. N. Tharrington (2011). "Implementing molecular dynamics on hybrid high performance computers-short range forces." Computer Physics Communications 182(4): 898-911. https://doi.org/10.1016/j.cpc.2010.12.021

Cao, Y., A. Taghvaie Nakhjiri and M. Ghadiri (2023). "Computational fluid dynamics comparison of prevalent liquid absorbents for the separation of SO_2 acidic pollutant inside a membrane contactor." Scientific Reports 13(1): 1300. https://doi.org/10.1038/s41598-023-28580-6

Daw, M. S. and M. I. Baskes (1984). "Embedded-atom method: Derivation and application to impurities, surfaces, and other defects in metals." Physical review B 29(12): 6443. https://

doi.org/10.1103/PhysRevB.29.6443

Daw, M. S., S. M. Foiles and M. I. Baskes (1993). "The embedded-atom method: a review of theory and applications." Materials Science Reports 9(7-8): 251-310. https://doi.org/10.1016/0920-2307(93)90001-U

Dukhan, N., Y.-c. K. Chen-Wiegart, A. P. y Puente, D. Erdeniz and D. C. Dunand (2020). "Introduction-porous metals: from nano to macro." Journal of Materials Research 35(19): 2529-2534. https://doi.org/10.1557/jmr.2020.282

Dokur, D., Keskin S. Effects of Force Field Selection on the Computational Ranking of MOFs for CO_2 Separations. Ind Eng Chem Res. 2018 Feb 14;57(6):2298-2309. https://doi.org/10.1021/acs.iecr.7b04792.

Fioletov, V., C. A. McLinden, D. Griffin, N. Theys, D. G. Loyola, P. Hedelt, N. A. Krotkov and C. Li (2020). "Anthropogenic and volcanic point source SO_2 emissions derived from TROPOMI on board Sentinel-5 Precursor: first results." Atmospheric Chemistry and Physics 20: 5591-5607. https://doi.org/10.5194/acp-20-5591-2020

Gao, X., G. Ji, J. Wang, L. Peng, X. Gu and L. Chen (2018). "Critical pore dimensions for gases in a BTESE-derived organic-inorganic hybrid silica: A theoretical analysis." Separation and Purification Technology 191: 27-37. https://doi.org/10.1016/j.seppur.2017.09.013

Gao, X., M. Qiu, K. Fu, P. Xu, X. Kong, X. Chen and Y. Fan (2018). "Feasibility analysis of SO_2 absorption using a hydrophilic ceramic membrane contactor." Chinese Journal of Chemical Engineering 26(10): 2139-2147. https://doi.org/10.1016/j.cjche.2018.07.011

Haile, J. M. (1992). Molecular dynamics simulation: elementary methods, John Wiley & Sons, Inc.

Hairer, E., C. Lubich and G. Wanner (2003). "Geometric numerical integration illustrated by the Störmer-Verlet method." Acta numerica 12: 399-450. https://doi.org/10.1017/S0962492902000144

Hilbert, S., P. Hänggi and J. Dunkel (2014). "Thermodynamic laws in isolated systems." Physical Review E 90(6): 062116. https://doi.org/10.1103/PhysRevE.90.062116

Hoover, W. G. (1985). "Canonical dynamics: Equilibrium phase-space distributions." Physical review A 31(3): 1695. https://doi.org/10.1103/PhysRevA.31.1695

Han, B., Cui, M., & Tong, R. (2025). Molecular dynamics simulation on friction properties of BCC iron strengthened by nanodiamonds. Molecular Simulation, 51(8), 529-545. https://doi.org/10.1080/08927022.2025.2507398.

Jolfaei, N. A., N. A. Jolfaei, M. Hekmatifar, A. Piranfar, D. Toghraie, R. Sabetvand and S. Rostami (2020). "Investigation of thermal properties of DNA structure with precise atomic arrangement via equilibrium and non-equilibrium molecular dynamics approaches." Computer methods and programs in biomedicine 185: 105169. https://doi.org/10.1016/j.cmpb.2019.105169

Jiang C, Wang X, Ouyang Y, Lu K, Jiang W, Xu H, Wei X, Wang Z, Dai F, Sun D. Recent advances in metal-organic frameworks for gas adsorption/separation. Nanoscale Adv. 2022 Mar 24;4(9):2077-2089. https://doi.org/10.1039/d2na00061j.

Kong, X., D. Gong, W. Ke, M. Qiu, K. Fu, P. Xu, X. Chen and Y. Fan (2020). "Investigation of mass transfer characteristics of SO_2 absorption into NaOH in a multichannel ceramic membrane contactor." Industrial & Engineering Chemistry Research 59(23): 11054-11062. https://doi.org/10.1021/acs.iecr.0c01327

Kong, X., M. Qiu, K. Fu, X. Gao, P. Xu, D. Gong, X. Chen and Y. Fan (2019). "Mass-transfer characteristics and optimization of a

hydrophilic ceramic membrane contactor for SO_2 absorption." Industrial & Engineering Chemistry Research 58(45): 20828-20837. https://doi.org/10.1021/acs.iecr.9b04641

Kuhn, H. and D. Medlin (2000). Mechanical testing and evaluation, ASM international.

Li, J. P. H. (2014). "Characterisation of Heterogeneous Acid/Base Catalysts and their Application in the Synthesis of Fine and Intermediate Chemicals." PhD diss., University of Newcastle, Australia.

Li, Z. G., X. E. Li and H. Y. Chen (2022). "Sulfur Dioxide: An Emerging Signaling Molecule in Plants." Frontiers in Plant Science 13: 891626. https://doi.org/10.3389/fpls.2022.891626

Liao, R., S. Wen, J. Liu, S. Bai and Q. Feng (2024). "Synergetic adsorption of dodecylamine and octyl hydroxamic acid on sulfidized smithsonite: Insights from experiments and molecular dynamics simulation." Separation and Purification Technology 329: 125106. https://doi.org/10.1016/j.seppur.2023.125106

Liu Y, Liu G, Zhang C, Qiu W, Yi S, Chernikova V, Chen Z, Belmabkhout Y, Shekhah O, Eddaoudi M, Koros W. Enhanced CO_2/CH_2 Separation Performance of a Mixed Matrix Membrane Based on Tailored MOF-Polymer Formulations. Adv Sci (Weinh). 2018 Aug 2;5(9):1800982. https://doi.org/10.1002/advs.201800982.

Ma, Y., T. Hua, T. A. Trinh, R. Wang and J. W. Chew (2022). "Molecular dynamics simulation of the competitive adsorption behavior of effluent organic matters by heated aluminum oxide particles (HAOPs)." Separation and Purification Technology 292: 120961. https://doi.org/10.1016/j.seppur.2022.120961

Martyna, G. J., D. J. Tobias and M. L. Klein (1994). "Constant pressure molecular dynamics algorithms." J. chem. Phys 101(4177): 10.1063.

Mayo, S. L., B. D. Olafson and W. A. Goddard (1990). "DREIDING: a generic force field for molecular simulations." Journal of Physical chemistry 94(26): 8897-8909. https://doi.org/10.1021/j100389a010

Mosavi, A., M. Hekmatifar, A. a. Alizadeh, D. Toghraie, R. Sabetvand and A. Karimipour (2020). "The molecular dynamics simulation of thermal manner of Ar/Cu nanofluid flow: the effects of spherical barriers size." Journal of Molecular Liquids 319: 114183. https://doi.org/10.1016/j.molliq.2020.114183

Nguyen, T. V., N. A. Luong, V. T. Nguyen, A. T. Pham, A. T. Le, T. L. To and V. Q. Nguyen (2021). "Effect of the phase composition of iron oxide nanorods on SO_2 gas sensing performance." Materials Research Bulletin 134: 111087. https://doi.org/10.1016/j.materresbull.2020.111087

Nosé, S. (1984). "A unified formulation of the constant temperature molecular dynamics methods." The Journal of chemical physics 81(1): 511-519. https://doi.org/10.1063/1.447334

Okwuashi, C. J. (2020). Molecular Dynamics Simulation of Nanoindentation and Nanoscratch of Silicon Wafer, Saint Louis University.

Pasichnyk, M., P. Stanovsky, P. Polezhaev, B. Zach, M. Šyc, M. Bobák, J. C. Jansen, M. Přibyl, J. E. Bara and K. Friess (2023). "Membrane technology for challenging separations: Removal of CO_2, SO_2 and NOx from flue and waste gases." Separation and Purification Technology 323: 124436. https://doi.org/10.1016/j.seppur.2023.124436

Plimpton, S. (1995). "Fast parallel algorithms for short-range molecular dynamics." Journal of computational physics 117(1): 1-19. https://doi.org/10.1006/jcph.1995.1039

Pourfayaz, F., H. Kazempour, M. Taheri and M. Mehrpooya (2025). "Simultaneous Optimization of Sulfur Recovery Efficiency and Thermal Energy Generation in the Catalytic

Section of the Sulfur Recovery Unit Simulated Based on Reaction Kinetics." ACS Omega 10(21): 21262-21279. https://doi.org/10.1021/acsomega.4c10709

Press, W., S. Teukolsky, W. Vetterling and B. Flannery (2007). "Section 17.4. Second-order conservative equations." Numerical recipes: The art of scientific computing, 3rd ed., Cambridge University Press, New York: 7.

Rapaport, D. C. (2004). The art of molecular dynamics simulation, Cambridge university press.

Sadus, R. J. (2002). Molecular simulation of fluids, Elsevier.

Singh, H., P. Saxena and Y. Puri (2021). "The manufacturing and applications of the porous metal membranes: A critical review." CIRP Journal of Manufacturing Science and Technology 33: 339-368. https://doi.org/10.1016/j.cirpj.2021.03.014

Syed Abdul Moiz Hashmi, Chong Yang Chuah, Euntae Yang, Wai Ching Poon, Advances in H2-selective metallic membranes for pre-combustion CO_2 capture: A critical review, Carbon Capture Science & Technology, Volume 13, 2024, 1000247, ISSN 2772-6568. https://doi.org/10.1016/j.ccst.2024.100247.

Soldemo, M. and J. Weissenrieder (2021). "Sulfur dioxide interaction with thin iron oxide films on low-index surfaces of iron." Surface Science 714: 121935. https://doi.org/10.1016/j.susc.2021.121935

Stukowski, A. (2009). "Visualization and analysis of atomistic simulation data with OVITO-the Open Visualization Tool." Modelling and simulation in materials science and engineering 18(1): 015012. https://doi.org/10.1088/0965-0393/18/1/015012

Thompson, A. P., H. M. Aktulga, R. Berger, D. S. Bolintineanu, W. M. Brown, P. S. Crozier, P. J. In't Veld, A. Kohlmeyer, S. G. Moore and T. D. Nguyen (2022). "LAMMPS-a flexible simulation tool for particle-based materials modeling at the atomic, meso, and continuum scales." Computer physics communications 271: 108171. https://doi.org/10.1016/j.cpc.2021.108171

Verlet, L. (1967). "Computer" experiments" on classical fluids. I. Thermodynamical properties of Lennard-Jones molecules." Physical review 159(1): 98. https://doi.org/10.1103/PhysRev.159.98

Wei, C.-C., F. Wu, G. Qu, K. Xiang and P. Ning (2024). "A critical review on the chelated-iron desulfurization process of fuel gas and the prospect of high value-added utilization of sulfur resources." Chemical Engineering and Processing: Process Intensification 201: 109819. https://doi.org/10.1016/j.cep.2024.109819

Xu, P., Y. Huang, X. Kong, D. Gong, K. Fu, X. Chen, M. Qiu and Y. Fan (2020). "Hydrophilic membrane contactor for improving selective removal of SO_2 by NaOH solution." Separation and Purification Technology 250: 117134. https://doi.org/10.1016/j.seppur.2020.117134

Xinyao Jiang and Maiyong Zhu, Metal-organic porous materials for gas adsorption: design principle for complex systems, Inorg. Chem. Front., 2025. https://doi.org/10.1039/D5QI01721A.

حذف انتخابی SO_2 از اکسیژن با استفاده از آهن متخلخل: مطالعه دینامیک مولکولی

- مصطفی جعفری[۱]، محمدمهدی یوسفی[۲]، علی وطنی[۳*]، روزبه ثابت وند[۴]

۱. پژوهشگر، انستیتو گاز طبیعی مایع، دانشکده مهندسی شیمی، دانشکده فنی، دانشگاه تهران، تهران، ایران

۲. دانشجوی کارشناسی ارشد، انستیتو گاز طبیعی مایع، دانشکده مهندسی شیمی، دانشکده فنی، دانشگاه تهران، تهران، ایران

۳. استاد تمام، انستیتو گاز طبیعی مایع، دانشکده مهندسی شیمی، دانشکده فنی، دانشگاه تهران، تهران، ایران

۴. دکترا، دانشکده مهندسی انرژی و فیزیک، دانشگاه صنعتی امیرکبیر، تهران، ایران

(ایمیل نویسنده مسئول: avatani@ut.ac.ir)

چکیـــــــده

دی‌اکسید گوگرد یک آلاینده سمی است که عمدتاً از احتراق سوخت‌های فسیلیِ حاوی گوگرد تولید می‌شود و حذف آن برای توسعه صنعتی پایدار حیاتی است. در این مطالعه محاسباتی، از شبیه‌سازی‌های دینامیک مولکولی (MD) برای ارزیابی یک غشای آهنی متخلخل به‌منظور جداسازی اکسیژن از جریان گازی SO_2 استفاده شد. غشای Fe با روش اتم نهفته (Embedded Atom Method, EAM) مدل‌سازی شد و مخلوط O_2–SO_2 با میدان نیروی DREIDING توصیف گردید. فرآیند برقراری تعادل، پایداری ساختاری مدل‌های اتمی را تأیید کرد که بازتاب‌دهنده تنظیمات مناسب MD و انتخاب دقیق شرایط اولیه بود. برای توصیف کارایی جداسازی، ضرایب جذب SO_2 و O_2، انرژی‌های برهم‌کنش گاز-غشاء و خواص مکانیکی غشاء پس از جداسازی گزارش می‌شوند. شبیه‌سازی‌ها همچنین نشان می‌دهند که شرایط اولیه (برای نمونه دما و فشار) رفتار جذب انتخابی غشاء متخلخل آهنی را در سراسر فرآیند شبیه‌سازی کنترل می‌کند. تحت شرایط بهینه، غشاء در سامانه پالایش در مقیاس اتمی به خلوصِ اکسیژن حدود ۸۱ درصد و بازیابی تقریب برابر با ۹۶/۷ درصد دست یافت. این عملکرد از برهم‌کنش بهینه میان غشاء متخلخل آهنی و مولکول‌های گاز هدف ناشی می‌شود. ازنظر عددی، قدر مطلقِ انرژی برهم‌کنش بین این نمونه‌های مدل شده به ۸۳/۱۴ eV- افزایش یافت. این فرآیند توصیف‌شده عملکرد مکانیکی غشاء طراحی‌شده را مختل نکرد و استحکام نهایی و مدول یانگ آن به ترتیب پس از تکمیل فرآیند جداسازی انتخابی به ۲۱۲/۳۹ MPa و ۶/۰۰ GPa رسید.

واژگان کلیدی: جداسازی O_2/SO_2، دینامیک مولکولی، خالص‌سازی گاز، فناوری غشاء اتمی، نفوذپذیری، گزینش‌پذیری اتمی، غشاء آهن متخلخل، خالص‌سازی در مقیاس اتمی